Characterization of Molecular Defects in Isovaleryl-CoA Dehydrogenase in Patients with Isovaleric Acidemia†

Al-Walid A. Mohsen,‡ Bambi D. Anderson,‡ Samuel L. Volchenboum,§ Kevin P. Battaile,§,|| Karen Tiffany,⊥ David Roberts,⊥ Jung-Ja P. Kim,⊥ and Jerry Vockley*,‡,§

Department of Medical Genetics, Department of Biochemistry and Molecular Biology, Mayo Clinic and Mayo Foundation, Rochester, Minnesota 55905, and Department of Biochemistry, Medical College of Wisconsin, Milwaukee, Wisconsin 53226

Received December 16, 1997; Revised Manuscript Received April 6, 1998

ABSTRACT: Isovaleryl-CoA dehydrogenase (IVD) is a homotetrameric mitochondrial flavoenzyme which catalyzes the conversion of isovaleryl-CoA to 3-methylcrotonyl-CoA. PCR of IVD genomic and complementary DNA was used to identify mutations occurring in patients with deficiencies in IVD activity. Western blotting, in vitro mitochondrial import, prokaryotic expression, and kinetic studies of IVD mutants were conducted to characterize the molecular defects caused by the amino acid replacements. Mutations leading to Arg21Pro, Asp40Asn, Ala282Val, Cys328Arg, Val342Ala, Arg363Cys, and Arg382Leu replacements were identified. Western blotting of fibroblast extracts and/or in vitro mitochondrial import experiments indicate that the seven precursor IVD mutant peptides, and a previously identified IVD Leu13Pro mutant, are synthesized and imported into mitochondria. While the IVD Leu13Pro, Arg21Pro, and Cys328Arg mutant peptides are rapidly degraded following mitochondrial import, the other mutant peptides exhibit greater mitochondrial stability, though less than the wild-type enzyme. Active IVD Ala282Val, Val342Ala, Arg363Cys, and Arg382Leu mutants were less stable than wild type when produced in *Escherichia coli*. The K_m values of purified IVD Ala282Val, Val342Ala, and Arg382Leu mutants are 27.0, 2.8, and 6.9 μM isovaleryl-CoA, respectively, compared to 3.1 μM for the wild type, using the electron-transfer flavoprotein (ETF) fluorescence quenching assay. The catalytic efficiency per mole of FAD content of these three mutants is 4.8, 17.0, and 17.0 $\mu M^{-1} \bullet min^{-1}$, respectively, compared to 170 $\mu M^{-1} \bullet min^{-1}$ for wild type.

Isovaleryl-CoA dehydrogenase (IVD;[1] EC 1.3.99.10) is a mitochondrial flavoenzyme which catalyzes the conversion of isovaleryl-CoA to 3-methylcrotonyl-CoA, the third step in the leucine catabolism pathway (*1, 2*). Deficiency of IVD activity in humans causes isovaleric acidemia (IVA), which can present with a widely variable clinical picture (*3*). IVD is a member of the family of acyl-CoA dehydrogenases (ACDs), which includes short/branched-chain acyl-CoA dehydrogenase (SBCAD), short-chain acyl-CoA dehydrogenase (SCAD), medium-chain acyl-CoA dehydrogenase (MCAD), long-chain acyl-CoA dehydrogenase (LCAD), and very long chain acyl-CoA dehydrogenase (VLCAD). These enzymes are encoded in the nuclear genome in precursor form. Precursor peptides are synthesized in the cytoplasm, transported into mitochondria, and processed to homotetramers (except VLCAD which is processed to a homodimer), with each monomer containing a noncovalently but tightly bound FAD molecule (*4, 5*). All ACDs catalyze the α,β-dehydrogenation of their corresponding acyl-CoA thio ester substrates, with each ACD having a distinct substrate specificity profile, and all transfer electrons to the electron transferring flavoprotein (ETF) (*6*−*8*).

In addition to their similarity in chemical function, the ACDs share 30−35% sequence homology within a species at the amino acid level, and the same ACD from different species share 85−90% sequence identity (*6, 9*−*12*). The three-dimensional structures of porcine MCAD, *Megalosphera elsdenii* butyryl-CoA dehydrogenase, and human IVD have also been reported to be similar (*13*−*15*). These primary and tertiary structure similarities make it possible to investigate the hypothetical importance of specific amino acid residues in the ACDs through molecular modeling. Conversely, naturally occurring point mutations, which significantly affect enzyme activity identified in patients with clinical deficiencies of the ACDs, establish the importance of specific amino acid residues for enzyme structure and/or function. Amino acid replacements in IVD, SCAD, MCAD, and VLCAD, leading to a variety of clinical presentations of the corresponding disorder, have been identified and

† This work was supported in part by Grants RO1-DK45482 (J.V.) and GM29076 (J.-J.P.K.) from the U.S. Public Health Service.

* To whom correspondence should be addressed.

‡ Department of Medical Genetics, Mayo Clinic and Mayo Foundation.

§ Department of Biochemistry and Molecular Biology, Mayo Clinic and Mayo Foundation.

|| Present address: Department of Molecular and Medical Genetics, Oregon Health Science University, L103, 3181 Sam Jackson Park Rd., Portland, OR 97201.

⊥ Department of Biochemistry, Medical College of Wisconsin.

[1] Abbreviations: ACD, acyl-CoA dehydrogenase; DCIP, dichlorophenolindophenol; CoA, coenzyme A; ETF, electron-transferring flavoprotein; FAD, flavin adenine dinucleotide; IPTG, isopropyl β-D-thiogalactoside; IVA, isovaleric acidemia; IVD, isovaleryl-CoA dehydrogenase; *IVD*, isovaleryl-CoA dehydrogenase cDNA or gene; LCAD, long-chain acyl-CoA dehydrogenase; MCAD, medium-chain acyl-CoA dehydrogenase; PMS, phenazine methosulfate; SBCAD, short/branched-chain acyl-CoA dehydrogenase; SCAD, short-chain acyl-CoA dehydrogenase; VLCAD, very long chain acyl-CoA dehydrogenase.

S0006-2960(97)03096-1 CCC: $15.00
Published on Web 06/20/1998

described (*9*, *16*−*21*). Two *IVD* nucleotide point mutations which have previously been identified in patients with IVA result in Leu13Pro or Gly170Val replacements (*21*). In this study, additional *IVD* point mutations responsible for causing IVA are reported, and biochemical properties of the IVD mutant proteins are described.

MATERIALS AND METHODS

Fibroblast Culture and Genomic and cDNA Isolation. Clinical description of IVA patients will be presented elsewhere. Patient fibroblast cells were grown in DMEM media from Gibco BRL (Grand Island, NY) supplemented with 10% fetal calf serum. Confluent cultures were harvested, and cell pellets were washed once in ice-cold 1.4 mM potassium phosphate/4.3 mM sodium phosphate/2.7 mM KCl/137 mM NaCl, pH 7.3, and then incubated for 12−18 h at 50 °C in 100 mM NaCl, 10 mM Tris-HCl, pH 8.0, 25 mM EDTA, 0.5% SDS containing 0.1 mg/mL proteinase K. Genomic DNA was precipitated with ethanol and sodium acetate and stored at −70 °C in 10 mM Tris-HCl, pH 8.0, 25 mM EDTA until use. mRNA was isolated from confluent fibroblast cultures using the QuickPrep kit according to the manufacturer's instructions (Pharmacia Biotech Inc., Piscataway, NJ). cDNA was synthesized using the *SUPERSCRIPT* Preamplification System for first-strand cDNA synthesis (Gibco BRL, Grand Island, NY).

Sequencing and Site-Directed Mutagenesis of the IVD cDNA. *IVD* DNA sequences were amplified from cDNA via the polymerase chain reaction as previously described (*21*). Amplified products were subcloned into pCR-Script SK(+) using the pCR-Script cloning kit according to manufacturer's instructions (Stratagene, LaJolla, CA). Clones isolated in this fashion were sequenced with Sequenase 2.0 and a 7-deaza-dGTP sequencing kit (US Biochemical, Cleveland, OH). At least six individual clones corresponding to each subcloned fragment of the *IVD* cDNA were sequenced to identify possible point mutations introduced during amplification. Alternatively, PCR-amplified fragments were sequenced directly by the Mayo Clinic molecular biology core facility using an ABI PRISM 377 DNA Sequencer unit (Perkin-Elmer, Foster City, CA). All mutations identified from IVD cDNA were confirmed to be present in genomic DNA by amplification of the appropriate segment of the IVD gene and sequencing of subcloned fragments or direct sequencing of the amplified fragments. Mutations identified in *IVD* cDNA from patient fibroblasts were then introduced into the prokaryotic expression vector pKm*HIVD*, containing an altered *IVD* cDNA designed for high expression (*22*). The mutations were introduced via PCR using mutagenic primers as previously described (*23*), or with the Muta-Gene mutagenesis kit according to the manufacturer's instructions (BioRad, Redmond, CA). Mutagenic primers were as follows (altered bases are underlined; note that some of the primers are in the antisense orientation; nucleotide position refers to precursor *IVD* sequence; see Tables 1 and 2 for the corresponding amino acid replacement): T125C, 5′-^{79}GAA TTC ATG CAC TCT CTG CTG CCG GTT GAC GAT GCT ATC AAC GGT C<u>C</u>G TCT GAA GAG^{135}-3′; G149C, 5′-^{12}CTG CAG GAA T<u>T</u>C ATG CAC TCT CTG CTG CCG GTT GAC GAT GCT ATC AAC GGT CTG TCT GAA GAG CAG CGT CAA CTG C<u>C</u>T CAG ACT ATG GCT A^{79}; G205A, 5′-^{79}AAG TTC CTG CAG GAA CAT CTG GCT CCG AAA GCT CAG GAG ATC <u>A</u>AT CGC AGC AAT GA^{34}-3′; G596T, 5′-^{421}GAC A<u>A</u>T CAG GAC GTC AGC ATC AGG G<u>A</u>C ATT AGT GAT CCA GAA CTT GTT^{474}-3′; C932T, 5′-^{869}GGC CTC TTG GGC TCA TGC AAG CGG TCC TGG ACC ACA CCA TTC CCT ACC TGC ACG TGA GGG AAG <u>T</u>CT TTG GCC AG^{943}-3′; T1069C, 5′-^{1079}ACA CCT GCA C<u>G</u>G TCC TTA GC^{1060}-3′; T1112C, 5′-^{1122}GTC CAG GGC T<u>G</u>C CTG TGT AG^{1103}-3′; C1174T, 5′-^{1184}CGA AGA AAG C<u>A</u>G CCC ATG GG^{1165}-3′. Note the sequence of the first three mutagenic primers corresponds to the altered 5′-end of the mature *IVD* expression vector. Mutations were introduced into the precursor form of human *IVD* cloned in the pTZ18U in vitro transcription/translation vector (BioRad) by subcloning. The T125C, G149C, and G205A nucleotide mutations were remade with primers corresponding to the wild-type *IVD* sequence (except that the desired mutation was included) rather than the modified prokaryotic expression vector. The G1232A mutation was constructed by subcloning the abnormal fragment amplified from patient cDNA directly into the wild-type IVD vectors. All mutant clones were sequenced in their entirety to ensure that only the desired mutation had been introduced into the IVD coding sequence.

Isolation of Rat Liver Mitochondria. Rat mitochondria were freshly prepared prior to each experiment as previously described with modifications (*24*). Briefly, a male Sprague-Dawly rat weighing approximately 150 g was sacrificed, and the liver was removed en bloc into cold 2 mM HEPES, pH 7.4, 220 mM D-mannitol, 70 mM sucrose (HMS buffer). The liver was diced and washed 3 times in HMS, and the pieces were placed in a Potter−Elvehjem homogenizer and homogenized by six up and down passes at progressively decreasing speeds. The homogenate was centrifuged at 3000*g* for 2 min, and the supernatant was further centrifuged for 6 min at 14500*g*. The final supernatant was removed and discarded, and the pellet was resuspended in 2 mL of HMS buffer and digested for 7 min with 3 mL of a 1.75 mg/mL digitonin solution (Fisher Scientific, Pittsburgh, PA). Twenty milliliters of HMS buffer was then added, and the suspension was centrifuged for 6 min at 14500*g*. The resulting pellet was washed once, and the final pellet was resuspended in 500 μL of HMS buffer. The concentration of mitochondria was determined as previously described and diluted to 30 mg/mL (*24*).

In Vitro Transcription/Translation and Mitochondrial Import of Normal and IVD Mutants. This was carried out to assess the stability of wild-type *IVD* and the various *IVD* mutant precursor cDNAs using rabbit reticulocyte lysate followed by import into freshly isolated rat mitochondria. Transcription and translation were carried out in the presence of [^{35}S]methionine (40 μCi, 10 Ci/μL; Amersham Life Sciences, Arlington Heights, IL) using the TnT Coupled Transcription/Translation kit according to the manufacturer's protocol (Promega Corp., Madison, WI). The DNA template for the reaction was either control or IVD mutant cloned into the pTZ18U vector under the control of the T7 promoter. After translation, 3 μL of translation product was set aside for analysis by western blotting. Each import assay was performed as follows: 60 μL of mitochondria in the HMS buffer was added to 120 μL of solution containing translation product, and then incubated at 30 °C for 30 min in the

presence of 15.6 μM unlabeled methionine. The mitochondria were then washed twice with 150 μL of HMS buffer, and the final mitochondrial pellet was resuspended in 23 μL of 10 mM potassium phosphate, pH 8.0, 0.5 mM EDTA, 1% Triton X-100, 0.4 mg/mL soybean trypsin inhibitor. Mitochondria were washed by centrifuging for 1 min at top speed in a microcentrifuge and resuspended in 200 μL of HMS buffer. Following three washes, the mitochondria were resuspended in 180 μL of buffer on ice. The mitochondria were incubated with 33 μg/mL trypsin for 10 min on ice followed by an additional 10 min incubation on ice after the addition of 5 μL of trypsin inhibitor (10 mg/mL). The mitochondria were then washed twice with 180 μL of HMS buffer, and finally resuspended in 180 μL of buffer. Forty microliters was removed (0 min time point), and the remaining 140 μL was returned to 30 °C. At 30 min, and 60 min, 40 μL aliquots were treated with 2% polyoxyxylene ethers W1 (Sigma, Inc., St. Louis, MO) to lyse mitochondria as previously described (*24*). The radioactive signal was visualized and quantified on a Molecular Dynamics PhosphorImager (Sunnyvale, CA) after an overnight exposure.

Prokaryotic Expression of Normal and Mutant IVDs. For prokaryotic expression experiments, pKm*HIVD* containing cDNA coding for the mature form of one of the various mutations was transfected into *E. coli* host strain XL Blue (Statagene, Inc.). Eight liter cultures in LB medium containing 50 μg/mL ampicillin were grown to an absorbency at 600 nm of 1 and induced for 1 h or overnight with 0.5 mM IPTG (Jersey Lab and Glove Supply, Livingston, NJ). Cells were harvested and disrupted by lysozyme treatment and sonication. Cell debris was removed by centrifugation, and enzymatic assays were performed on the supernatant. The protein concentration of the supernatants was determined using the BioRad DC Protein Assay Kit (Redmond, CA). For western blotting, 50 mL cultures were grown to an absorbency at 600 nm of 1 and induced for 1 h or overnight with 0.5 mM IPTG. One milliliter of cells was centrifuged to a pellet at top speed in a microfuge, resuspended in 100 μL of SDS−PAGE sample buffer, and boiled for 5 min. Two microliters of this sample was used for SDS−polyacrylamide gel electrophoresis (*25*). A cytoplasmic extract was made from the remainder of the culture as described below, an aliquot of which was used for Western blotting experiments.

Purification of Wild-Type and Mutant IVDs. This was performed as described (*22*), with modifications to improve the yield of less stable mutant proteins. The supernatant from an induced culture was loaded onto an XK16/20 Fast Q fast flow column, washed with 10 mM Tris, pH 7.5, and eluted with a 120 mL gradient of 0−300 mM NaCl in 10 mM Tris, pH 7.5. Following overnight dialysis in 10 mM potassium phosphate buffer, pH 7.4, the sample was loaded onto a 10 × 30 cm 10 μm ceramic hydroxyapatite column in 10 mM potassium phosphate buffer, pH 7.4, and eluted with a 650 mL gradient of 50−175 mM potassium phosphate, pH 7.4. Fractions were monitored for absorbency at 445 and 270 nm, and the middle half of the maximum 445/270 nm ratio peak was concentrated to 1−2 mL in a Centricon-30, diluted to 15 mL with water, and concentrated to 2 mL again. The final sample was brought to 20% glycerol and stored at −80 °C in 500 μL aliquots until use.

Enzyme Assays and Western Blotting. Enzyme activity was determined using the anaerobic ETF fluorescence quenching assay with 50 μM isovaleryl-CoA (from Sigma) as substrate as previously described (*23*, *26*). One unit is defined as the amount of enzyme necessary to completely reduce 1 μmol of ETF in 1 min. For kinetic analyses, ETF concentration was kept constant at 1 μM, and the isovaleryl-CoA concentration was varied from 1 to 50 μM; k_m and V_{max} were calculated on a Macintosh computer using the UltraFit software package from Biosoft (Ferguson, MO). Catalytic efficiency per FAD was calculated using the flavin content estimated with the absorbency of the purified enzyme at $\lambda_{445\ nm}$ and the molar extinction coefficient determined for purified recombinant IVD ($\epsilon_{445\ nm} = 13.9\ mM^{-1}\ cm^{-1}$). Western blotting of fibroblast extracts and the *E. coli* cell supernatants following SDS−PAGE was performed as previously described using a 1:500 dilution of a rabbit antiserum raised to the purified recombinant human IVD as a primary antibody (*22*). Visualization was with alkaline phosphatase-conjugated goat anti-rabbit IgG antibodies as previously described (*27*). Membrane images were digitized into a personal computer using a ScanMaker 600ZS image scanner from Microtek International, Inc. (Hsinchu, Taiwan), and band intensities were quantified with the Image 1.6 software (NIH, Research Services Branch).

Monitoring the Formation of the Charge-Transfer Complex. Productive formation of the charge-transfer complex was monitored by observing the increase in absorbency at 580 nm with the concomitant decrease in absorbency at the 445 nm region. Spectral scans were performed using a DU7400 spectrophotometer from Beckman (Palo Alto, CA) as previously described (*28*). Briefly, IVD protein was diluted in a quartz cuvette to give a concentration of approximately 2 nM FAD, in 500 μL of 10 mM potassium phosphate, 0.1 mM EDTA, 10% glycerol, pH 8.0, and the cuvette was sealed with a rubber stopper. The IVD sample was then subjected to 10, 40 s cycles of vacuum purging alternating with dry, oxygen-free argon. Increasing amounts of substrate were sequentially added using a Hamilton syringe to the cuvette, and spectral scans were performed from 240 to 700 nm after each addition. Substrate concentrations used were 0.75, 1.5, 2.2, 3.0, 3.7, 5.5, 7.3, 9.1, 10.8, 12.5, 14.2, 20.7, and 26.8 μM (given as the final concentration of substrate in the cuvette after the most recent addition) for wild-type IVD and the IVD Ala282Val and Val343Ala mutants. Isovaleryl-CoA concentrations used for the Arg382Leu mutant were 1.5, 3.0, 4.5, 6.0, 7.5, 8.9, 10.4, 11.9, 13.4, 14.9, 16.4, 17.9, 19.4, 20.9, 25.9, 30.9, 35.9, 40.9, 45.9, and 50.9 μM. Data from the scans were analyzed using the UltraFit software package from Biosoft. Changes in absorbency values at 445 nm were plotted as a function of substrate concentrations, and a value K_f (where K_f is the substrate concentration which induces half the maximum quenching of the absorbency in the 445 nm region) was then calculated using a nonlinear regression algorithm (*28*).

Molecular Modeling of IVD Mutations. The three-dimensional structure of IVD crystals (Brookhaven Protein Data Bank, identification code 1IVH) was visualized using an Insight II 95.5 package of modeling software from Molecular Simulations, Inc. (San Diego, CA), and a Silicon Graphics Indigo 2 Extreme workstation (Mountain View, CA).

Table 1: Mutations Identified in Fibroblast Cell Lines of Patients with Isovaleric Acidemia

cell line[a] designation	allele 1[b]	allele 2[b]
YH 501[c]	T125C (Leu13Pro)	unknown
FB 118	G149C (Arg21Pro)	G149C (Arg21Pro)
FB 103	G205A (Asp40Asn)	intron 4 splice acceptor site mutation
YH 834[c]	G596T (Gly170Val)	intron 1 insertion/splicing mutation
FB 102	C932T (Ala282Val)	intron 7 splice acceptor site mutation
FB 2368	T1069C (Cys328Arg)	C1174T (Arg363Cys)
FB 1322	T1112C (Val342Ala)	frameshift (deletion of nucleotide 618)
FB 104	G1232A (Arg382Leu)	G1232A (Arg382Leu)

[a] No molecular defect has been identified for cell line FB 1339 despite the presence of apparently normal *IVD* mRNA in the cytoplasm (*21*). [b] Capital letters and numbering refer to the nucleotide and its position in precursor cDNA. In parentheses are resulting amino acid replacements with all numbering in terms of the mature enzyme. A study of mutations identified in noncoding regions in the *IVD* gene will be published elsewhere. [c] See earlier published report (*21*).

RESULTS

Mutation Analysis of IVA Patients' Fibroblasts. The nucleotide point mutations and the corresponding predicted amino acid replacements identified in patient cell lines are listed in Table 1, and their locations in the monomer's three-dimensional model are depicted in Figure 1. In all cases, point mutations in the cDNA were confirmed in genomic cDNA from the cell line. YH 501 is a cell line which has previously been shown to encode a nucleotide point mutation (T125C) on one allele, while the other allele is not expressed or leads to the synthesis of an unstable RNA species (*21*). YH 834 also has previously been shown to be a compound mutant with one allele containing a G596T nucleotide point mutation and a second encoding an RNA species that is improperly spliced (*21*). In this study, only one (FB 2368) of the eight cell lines studied was found to be a compound mutant for two point mutations in coding regions, while two (FB 104 and FB 118) are homozygous for a single point mutation. The remaining cell lines express only one *IVD* message capable of synthesizing a full-length IVD subunit.

IVD Activity and Its Presence in IVA Patients' Fibroblasts. Fibroblast extracts, except YH 501, were assayed for IVD activity with the ETF fluorescence quenching assay. IVD activity, only detected in one fibroblast cell line (FB 102, harboring the mutation corresponding to the IVD Ala282Val mutant), was 0.34 ± 0.07 ($n = 3$) nmol of ETF•min^{-1}•(mg of protein)$^{-1}$ compared to 4.1 ± 0.6 ($n = 3$) nmol of ETF•min^{-1}•(mg of protein)$^{-1}$ in normal human fibroblast cells. Extracts from the other cell lines, including the FB 104 fibroblast cell line which has the highest Western blot signal (see below), have no detectable IVD activity.

Extracts from fibroblast cells harboring the IVD Arg382Leu mutant (FB 104) had an IVD immunoblot band of 80% in intensity compared to the normal cell line (Figure 2, lane 7). The IVD mutant bands detected from FB 102 (Ala282Val), YH 834 (Gly170Val), and FB 1322 (Val342Ala) were approximately half the intensity of the wild-type signal (Figure 2, lanes 3−5). The IVD signals from FB 103 (Asp40Asn) and FB 2368 (containing the Cys328Arg and Arg363Cys replacements on different alleles) extracts are approximately 10% and 20% of the intensity of the IVD signal in normal cells, respectively (Figure 2, lanes 6 and 8). The fibroblast extracts from the cell lines FB 1339 (*18*) and FB 118 (Arg21Pro) contain no immunodetectable IVD protein (Figure 2, lanes 2 and 9).

Mitochondrial Import and Stability of IVD Mutants. Figure 3 shows the radioactive IVD bands as detected by the PhosphorImager. To quantify the mitochondrial stability of the IVD mutant peptides, the ratio of the amount of radioactive IVD mutant present after an hour incubation at 30 °C as compared to a concurrent wild-type sample was calculated (Table 2). A wild-type IVD sample was included with each import experiment to correct for relative import efficiency among the various experiments. About 70% of newly imported wild-type IVD is still present in isolated mitochondria 30 min after import with incubation at 30 °C, and about 45% is present after 1 h, as estimated digitally by the PhosphorImager.

The amount of IVD Ala282Val and Val342Ala mutants detected following mitochondrial import compared to wild type is consistent with results from the Western blots of fibroblast cell extracts from patients with the corresponding defects (see above). The signals of the IVD Asp40Asn and Arg382Leu mutants in mitochondria are not significantly different. The IVD Asp40Asn mutant is more stable following import into mitochondria using the in vitro system compared to the estimated Western blot signal in corresponding patient fibroblast cells (see above). The Western blot signal of IVD Arg363Cys following import is weaker than the other mutants discussed above. The IVD Leu13Pro, Arg21Pro, and Cys328Arg mutant Western blot signals of the mature protein are similar in intensity, but much weaker compared to the other mutants following import into mitochondria. In contrast to all other IVD mutants, the IVD Gly170Val mutant precursor peptide was undetectable following in vitro transcription/translation (Figure 3).

E. coli Expression of IVD Mutant cDNAs. Individual *IVD* cDNA mutants were expressed in *E. coli*. Following induction with IPTG, whole cells and extracts of the bacterial cultures were analyzed for the presence of IVD protein by SDS−PAGE and Western blotting, and compared to the amount of total wild-type IVD protein produced under the same conditions (Figure 4). A low level of soluble IVD production is evident in preinduced cells containing the wild-type *IVD* plasmid which increases dramatically with induction, while no IVD protein signal is seen with induction of cells containing the parent plasmid without an *IVD* insert.

The IVD Ala282Val, Val342Ala, Arg382Leu, Arg21Pro, Asp40Asn, and Arg363Cys mutants are detected in Western blots of the supernatant fraction. The Western blot signals of these mutants are similar to that of the wild-type IVD following induction. The IVD Gly170Val and Cys328Arg mutant proteins are barely detectable in crude cell extracts from cells induced overnight. Following a 1 h induction, these proteins can be identified at a higher level in cell extracts (not shown); however, the IVD Gly170Val and Cys328Arg mutant proteins are present in significant quantities in whole cells, though less than for the wild-type IVD case.

Production of the recombinant IVD Leu13Pro mutant is the lowest among all the IVD mutants as evident from its weak Western blot signal in whole cells and its absence from

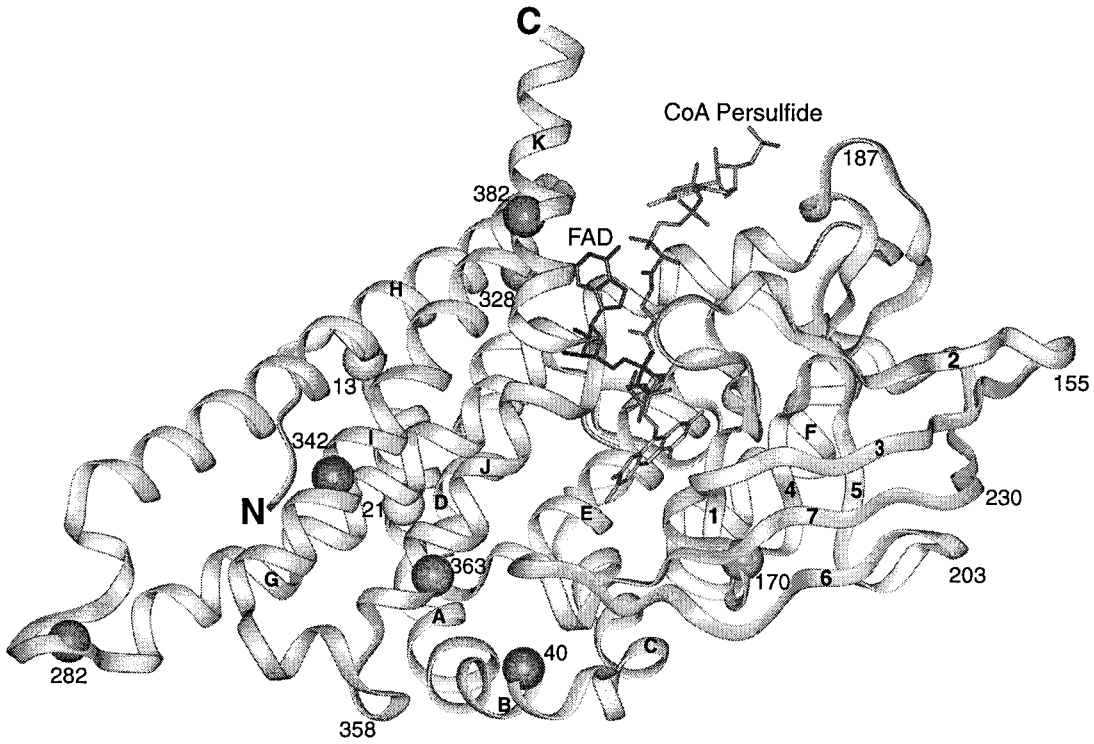

FIGURE 1: Ribbon diagram of a monomer of human IVD with bound CoA persulfide depicting the locations of the amino acid replacements, which were identified in patients with isovaleric acidemia, with dark and light shaded balls. The light shaded balls (Leu13 and Arg21) are located at the backside of the molecule. The atomic coordinates of the human IVD tetramer are deposited in the Brookhaven PDB with the identification code 1IVH (*15*).

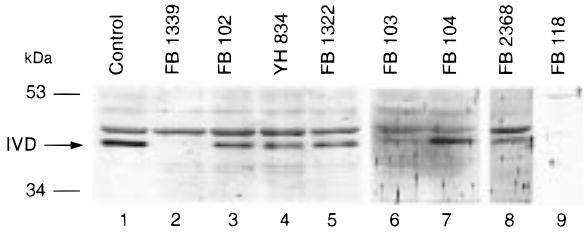

FIGURE 2: Western blotting of IVA patients' fibroblasts. Western blotting of extracts from fibroblasts of patients with isovaleric acidemia was performed as described under Materials and Methods. Western blotting of an SDS−polyacrylamide gel with 43 (lanes 1−5) or 50 μg (lanes 6−10) of fibroblast extract protein loaded in each sample lane. The gel was probed with a rabbit anti-human IVD antiserum. Lane 1, control diploid fibroblast cell line ConH. Lane 2, FB 1339, an IVA cell previously shown not to express immunoreactive IVD protein. Lanes 3−9, IVA fibroblast cell lines containing point mutations as described in the text. The migration position of purified IVD is marked with an arrow. The prestained molecular mass markers are 48.3 kDa (ovalbumin) and 33.4 kDa (carbonic anhydrase).

the *E. coli* supernatant (Figure 4, lane 6). However, the soluble Leu13Pro protein is present at higher concentrations following an hour induction than in the overnight sample (not shown), which is consistent with production of an unstable protein that subsequently aggregates. The cytoplasmic presence in *E. coli* was not improved by the coexpression of bacterial GroEL/ES (data not shown), which has successfully been used to stabilize other mutant ACDs when expressed in *E. coli* (*29*).

IVD Activity of the Recombinant Mutants in E. coli Extracts. IVD activity was examined in *E. coli* cell-free extracts using the ETF fluorescence quenching assay. Extracts of cells containing vector without the wild-type *IVD* cDNA insert give no detectable IVD activity. When the wild-type *IVD* cDNA insert is present, IVD activity is detected at a level of 0.44 unit/mg of protein of induced cell extract measured with the ETF fluorescence assay, corresponding to a concentration of 2.3 mg of IVD/mL of sample (Table 3). The recombinant IVD Ala282Val, Val342Ala, and Arg382Leu mutants have significant enzyme activity in crude extracts. The recombinant IVD Ala282Val mutant has the highest activity in the crude extract among all the mutants. The recombinant IVD Arg363Cys mutant shows detectable activity although its activity is significantly less than the others.

E. coli extracts of cells expressing *IVD* mutant cDNAs coding for the Arg21Pro or Asp40Asn mutants show no detectable activity even when 10 000 times more total soluble cellular protein than has been used for wild-type assays is added to the assay mix. This is despite the significant presence of soluble forms of these mutants as evident from the Western blot data. As expected, extracts of cells expressing *IVD* cDNAs coding for the Leu13Pro, Gly170Val, and Cys328Arg mutants, which show the weakest Western blot signals, do not show any detectable activity using similar high quantities of cellular protein as above.

Purification of IVD Mutants. Four active IVD mutants have been purified or partially purified for further analysis. Because of their low yields, our previously published protocol for purification of IVD produced in *E. coli* (*22*) was modified, substituting a Mono Q anion exchange column for the DEAE-Sepharose and using a steeper elution gradient. This procedure yields a wild-type IVD preparation that is approximately 95% pure as judged by densitometric scanning (Figure 5, lane 1). Yields during purification of the mutant proteins are significantly lower than for the wild-type enzyme. Preparations of the IVD Ala282Val and Val342Ala

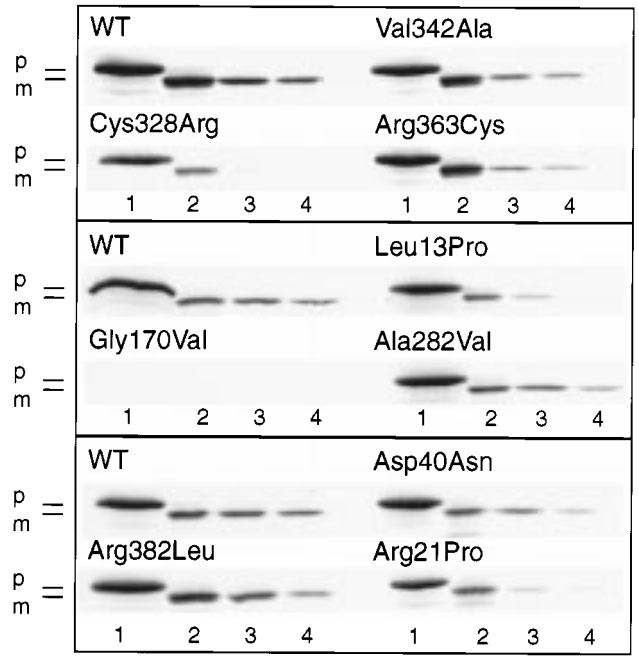

FIGURE 3: Mitochondrial import of IVD wild type and mutants following in vitro transcription/translation. The precursor coding sequences for control and mutant IVDs were transcribed and translated and then imported for 30 min into rat liver mitochondria as described under Materials and Methods. Following removal of unimported precursor, the samples were incubated for an additional 30 or 60 min, and then processed for electrophoresis on SDS−PAGE gels. The radioactive signals following electrophoresis were visualized and quantitated with a PhosphorImager. The migration position of precursor (p) and mature (m) forms of wild-type IVD are marked on the figure. Each box represents a separate experiment, all of which included a concurrent wild-type IVD control. The mutant being tested is listed above the precursor product lane. Lanes 1, translation product (precursor); lanes 2, imported protein following trypsinization of unimported precursor IVD; lanes 3 and 4, 30 and 60 min, respectively, incubation at 32 °C after removal of unimported precursor.

Table 2: Relative Mitochondrial Stability[a] of IVD Mutants

enzyme	relative stability (%)	enzyme	relative stability (%)
wild type	100	Val342Ala	60
Leu13Pro	13	Cys328Arg	14
Arg21Pro	16	Arg363Cys	39
Asp40Asn	42	Arg382Leu	41
Ala282Val	55		

[a] Stability is defined as the percentage of the amount of the radioactive IVD mutant present in the mitochondrial matrix, after 1 h incubation at 30 °C post import, relative to that of the wild type.

mutants are >90% pure (Figure 5, lanes 2, 3). Although the purified IVD Ala282Val, Val342Ala, and Arg382Leu mutants were active, their yields were low, indicating that their structural integrity was adversely affected by the amino acid replacement compared to the wild type.

The Arg382Leu protein behaves abnormally on elution from the hydroxyapatite column. A fraction with enzyme activity containing predominantly IVD elutes at the phosphate concentration where wild-type protein elutes (Figure 5, lane 4). An additional IVD fraction which lacks detectable FAD elutes at a slightly higher phosphate concentration than wild-type IVD, which is characteristic of the other IVD mutants eluted as well. This fraction is also predominantly IVD protein as determined by SDS gel electrophoresis

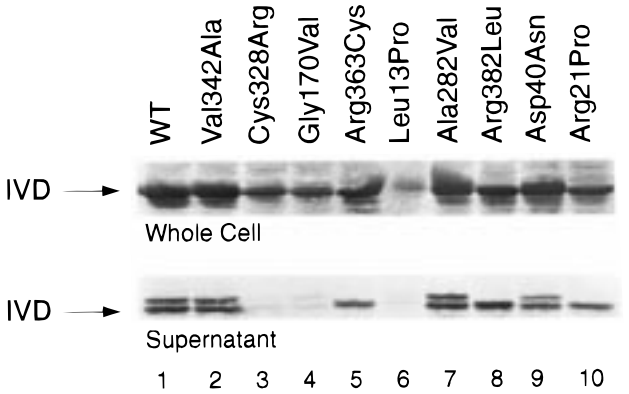

FIGURE 4: Western blotting of IVD mutants expressed in *E. coli*. IVD mutations were introduced into the mature IVD coding sequence in an *E. coli* expression vector as described under Materials and Methods. Mid-log cultures were induced overnight at 37 °C, and an aliquot of the culture or cell free extract was prepared for electrophoresis on SDS−PAGE gels as described. The proteins were transferred to a PVDF membrane and probed with a rabbit anti-human IVD antiserum. The top portion of the figure shows whole cell samples, while the bottom shows a crude cell extract supernatant fraction. Lane 1, wild-type pKm*HIVD* plasmid. Lanes 2−10, expression of mutant IVD cDNAs as described in the text. The migration position of purified wild type IVD is indicated with an arrow. For whole cells, the top band of a darkly staining doublet comigrated with pure IVD. For cell supernatant, a protein which migrated slightly slower than IVD was often visualized.

Table 3: Enzyme Activity Measured in Cell-Free Extracts of *E. coli* Cells Expressing Human *IVD* CDNA Mutants

cDNA mutation	amino acid[a]	IVD specific activity[b]	% wild-type activity
wild type	wild type	440 ± 66	100
T125C	Leu13Pro	ND[c]	0
G149C	Arg21Pro	ND[c]	0
G205A	Asp40Asn	ND[c]	0
G596T	Gly170Val	ND[c]	0
C932T	Ala282Val	86 ± 2	19
T1069C	Cys328Arg	ND[c]	0
T1112C	Val342Ala	52 ± 8	12
C1174T	Arg363Cys	4 ± 2	1
G1232A	Arg382Leu	32 ± 2	7

[a] Expressed in mature protein numbering. [b] Specific activity ± standard deviation ($n = 3$) of IVD in crude lysate; expressed as nmol of ETF reduced•min^{-1}•mg of protein^{-1}. [c] Not detectable.

(Figure 5, lane 5), but has no measurable IVD activity. Approximately 10% of the IVD Arg382Leu mutant protein elutes with the earlier fraction while the remainder appears in the later fraction. The two fractions are approximately of the same purity as estimated from SDS−PAGE.

The IVD Arg363Cys mutant protein was more difficult to purify than wild type, but a small amount of partially purified protein was obtained (Figure 5, lane 6). The Arg21Pro and Asp40Asn mutant enzymes did not survive the anion exchange step even when glycerol or polyethylene glycol was added to all buffers.

Table 4 shows specific activity measurements for the wild-type and recombinant IVD mutants using the ETF fluorescence quenching or the PMS/DCIP assay with 50 μM isovaleryl-CoA present as substrate. The mutant enzymes show considerably less specific activity than wild type. Furthermore, their specific activities are similar using either electron acceptor. Preincubation of enzyme samples with

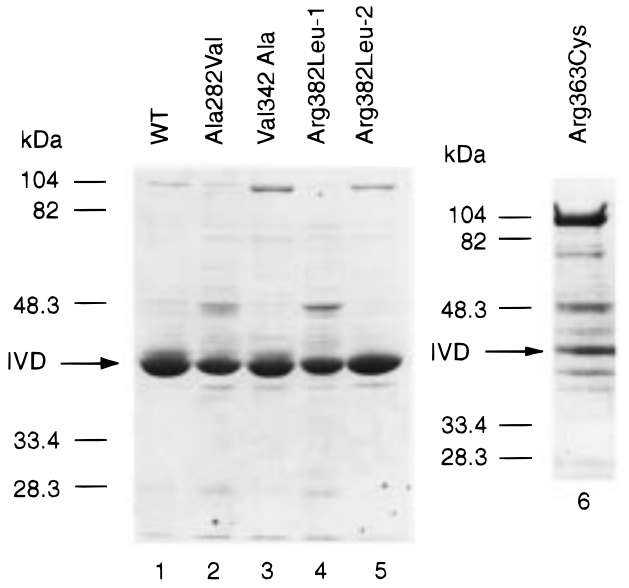

FIGURE 5: Purification of wild-type and mutant IVDs. Purified fractions of wild-type and mutant IVDs produced in *E. coli* were separated on a 10% SDS−PAGE gel and stained with Coomassie blue as described. (Left panel) Lane 1, wild-type IVD; lane 2, Ala282Val mutant; lane 3, Val342Ala mutant; lane 4, Arg382Leu first hydroxyapatite peak; lane 5, Arg382Leu second hydroxyapatite peak. Migration positions of prestained molecular mass markers are indicated on the left of the figure and are 104 kDa (phosphorylase B), 82 kDa (bovine serum albumin), 48.3 kDa (ovalbumin), 33.4 kDa (carbonic anhydrase), and 28.3 kDa (soybean trypsin inhibitor). The arrow indicates the migration of a previously purified preparation of wild-type IVD. (Right panel) Arg363Cys mutant. The molecular mass markers to the left of the lane are the same as in the left panel.

Table 4: Specific Activity[a] of Purified Recombinant Human IVD Mutants

	electron acceptor		
mutant	ETF	DCIP	DCIP + FAD
wild type	11.7	8.20	10.30
Ala282Val	2.2	2.04	2.33
Val342Ala	0.6	1.27	1.24
Arg382Leu[b]	1.4	4.88	6.34

[a] Activities were measured using ETF or DCIP as a final electron acceptor. Reactions with DCIP as electron acceptor were performed with and without added FAD. Specific activity is expressed as μmol of final electron acceptor reduced•min^{-1}•mg of protein^{-1}. [b] Kinetic parameters for IVD Arg382Leu eluted with detectable bound FAD.

FAD results in only slightly higher activity for the wild-type IVD, the Ala282Val mutant, or the first hydroxyapatite fraction of the Arg282Leu mutant (17, 10, and 23%, respectively). This procedure has previously been reported to reconstitute active holoenzyme from FAD-deficient apoenzyme (*30*). The activities of the IVD Val342Ala mutant and the latter hydroxyapatite fraction of IVD Arg282Leu are unchanged using the PMS/DCIP assay when preincubated with FAD. The partially purified (approximately 40% pure) IVD Arg363Cys mutant activity cannot be measured with PMS/DCIP even when the mutant is preincubated with FAD, but some activity can be detected [0.01 μmol of ETF•min^{-1}•(mg of protein)$^{-1}$] using the ETF fluorescence quenching assay.

Spectral Analysis of IVD Mutants. Spectral scans of the purified IVD mutants are shown in Figure 6. The wild-type spectrum without added substrate is similar to that obtained in previous studies (*23*). The spectral maximum absorbencies of IVD in the presence of bound CoA persulfide are at 267, 361, and 442 nm. In addition, a spectral band at the 650−700 nm wavelength region could be observed at higher enzyme concentrations, which is characteristic of the presence of a tightly bound CoA persulfide (*31*). The presence of this spectral band, however, has been inconsistent among various preparations. When this absorbency band is present, the ratio of A_{700}/A_{442} is approximately 0.1.

The IVD Ala282Val mutant spectrum has a maximum at 277 nm with a broad shoulder extending to 365 nm and a second maximum at 430 nm. The IVD Val342Ala mutant has maximum absorbency at 270, 358, and 430 nm. The earlier hydroxyapatite fraction of the Arg382Leu mutant has maximum absorbency which is similar to the former two mutants (Figure 6). However, the characteristic FAD maximum absorbency at 367 and 445 nm of the later hydroxyapatite fraction cannot be distinguished at a protein concentration of 3.3 mg•mL^{-1} (not shown), indicating significant loss of FAD. The remaining mutant enzymes have spectra that differ from wild type, reflecting a significant loss of FAD and perturbation of the binding of the remaining FAD to the protein. The Arg363Cys mutant enzyme (which was only partially purified) shows a broad maximum absorbency at wavelengths longer than 277 nm, but a typical FAD spectral pattern was not apparent (data not shown).

To assess the ability of the purified IVD mutants to interact with the bona fide substrate, absorbency spectra of wild-type IVD and IVD mutants were monitored at various isovaleryl-CoA concentrations, and the substrate concentration which induces half the maximum quenching of the absorbency at 430−445 nm (K_f) was calculated (Figure 6). The K_f for the wild-type IVD is 1.5 μM isovaleryl-CoA. The decrease in absorption at 445 nm area is accompanied by a blue shift to 436 nm and is paralleled by development of the long-wavelength band characteristic of the charge-transfer complex.

The IVD Ala282Val and Arg382Leu mutants show a slight red shift in their peak absorbency at the 445 nm region in the presence of isovaleryl-CoA (Figure 6). A decrease in the absorbency along the whole 320−700 nm region was observed in the IVD Ala282Val mutant scans in the presence of the substrate. The isovaleryl-CoA concentration required to induce half-maximal quenching at the 445 nm region for this mutant is 9.0 μM. The IVD Val342Ala scans in the presence of saturating concentrations of isovaleryl-CoA show a reduction of the flavin absorbency at the 445 nm region with a concomitant increase in the absorption at 580 nm. However, a large excess of isovaleryl-CoA was able to quench the absorbency at the 445 nm region only slightly for this mutant. In contrast, the IVD Arg382Leu mutant scans show a minor red shift of the 445 nm peak region in the presence of substrate.

Kinetic Properties of Purified Recombinant IVD Mutants. Kinetic properties of the purified wild-type and IVD mutants were monitored using the ETF fluorescence quenching or the PMS/DCIP colorimetric assays (Table 5). All of the purified mutant enzymes show lower catalytic efficiency compared to wild-type IVD using both assays. The IVD Ala282Val mutant kinetic data show that the K_m is 9 times higher, the V_{max} is 4 times higher, and the catalytic efficiency

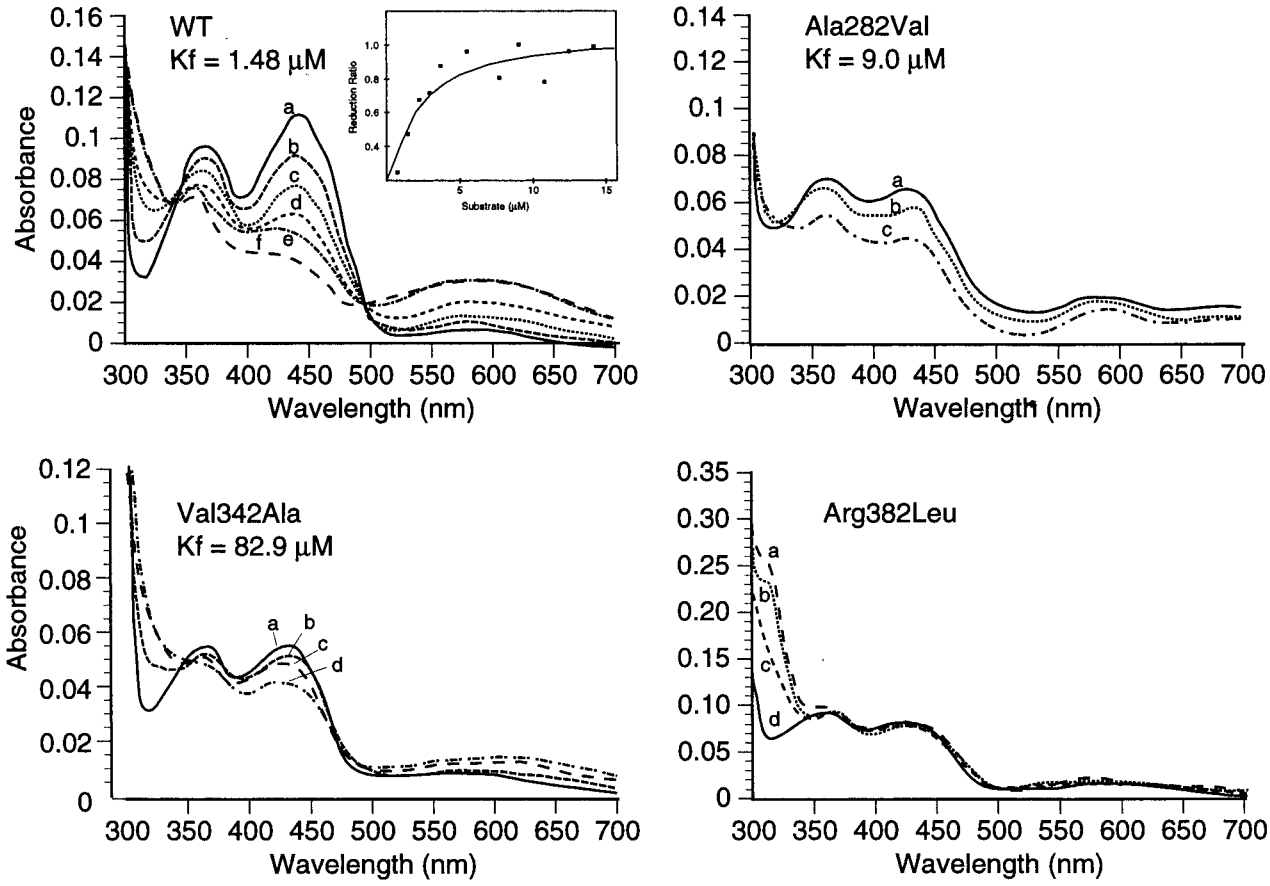

FIGURE 6: Quenching of flavin absorption by addition of isovaleryl-CoA to wild-type and mutant IVDs. Purified wild-type and mutant IVDs were diluted in a quartz cuvette to an absorbency of 0.05−0.1 at the 430−450 nm maximum, molecular oxygen was removed as before, and the sample was scanned from 240 to 700 nm wavelength. Isovaleryl-CoA was added sequentially under anaerobic conditions as indicated in the text. Graphs of absorbency vs wavelength for wild-type (WT) IVD and the Ala282Val, Val342Ala, and Arg382Leu (first hydroxyapatite fraction) mutants are shown. Only scans from selected substrate concentrations are shown for clarity sake. In each graph, (a) corresponds to the sample scanned without added substrate. The remaining scans shown are as follows: for WT, b, 0.75 μM; c, 1.5 μM; d, 3.7 μM; e, 7.3 μM; f, 14.2 μM final substrate concentration: for Ala382Val, b, 3.0 μM; c, 53.7 μM final substrate concentration; for Val343Ala, b, 3.7 μM; c, 14.2 μM; d, 25.5 μM final substrate concentration; for Arg382Leu, b, 3.0 μM; c, 14.2 μM; d, 53.7 μM final substrate concentration. The inset in the wild-type IVD graph shows the reduction ratio (defined as reduction of the flavin peak at a substrate concentration as a ratio of the maximum reduction of that peak). The substrate concentration required to achieve half-maximal reduction of the peak (K_f) was calculated from this graph and is listed underneath the enzyme name. Similar calculations were performed for the Ala282Val and Val342Ala mutant enzymes. The change in absorbance upon substrate addition to the Arg382Leu mutant IVD was not great enough to quantify.

Table 5: Kinetic Parameters of Recombinant Human IVD Mutants Measured Using the ETF Fluorescence Quenching or the PMS/DCIP Assays

	wild type		mutant					
			Ala282Val		Val342Ala		Arg382Leu[a]	
	ETF	DCIP	ETF	DCIP	ETF	DCIP	ETF	DCIP
amount of enzyme used (μg)	0.07	17.0	1.0	10.4	1.1	22.0	0.5	11.0
K_m (μM)	3.1	29.6	27.0	410	2.8	24.0	6.9	4.5
V_{max} (nmol of ETF•min^{-1})	0.82	9.3	2.3	30.6	0.61	4.3	0.77	5.6
K_{cat} per mol of FAD (s^{-1})	8.8	10.0	2.2	2.81	0.81	0.29	2.0	0.73
tetramer catalytic efficiency (μM^{-1}•min^{-1})	520	61.8	11.4	1.0	27	1.1	28	15.5
catalytic efficiency per mol of FAD (μM^{-1}•min^{-1})	170	20.4	4.8	0.4	17	0.73	17	9.6

[a] Kinetic parameters for IVD Arg382Leu which eluted with detectable bound FAD.

is 35 times lower compared to the wild type using the ETF fluorescence quenching assay. Results using the PMS/DCIP assay are similar. In contrast, the IVD Val342Ala mutant shows similar K_m values to the wild-type enzyme using either the ETF or the PMS/DCIP assays, while the decrease in subunit catalytic efficiency is only 10-fold compared to the wild type. The FAD containing fraction of IVD Arg382Leu has a higher K_m and similar V_{max} as compared to wild-type enzyme when measured with ETF fluorescence quenching assay. The specific activity, as measured by the PMS/DCIP assay, increases by 20% when the mutant is preincubated with FAD. The K_m of the IVD Arg382Leu is significantly lower using the PMS/DCIP assay compared to that measured with the ETF fluorescence quenching assay. The magnitude of the decrease in the subunit catalytic efficiency resulting from the Arg382Leu replacement is more pronounced using the ETF fluorescence quenching assay compared to the decrease using the PMS/

DCIP assay. The latter IVD Arg382Leu fraction deficient in FAD content has barely detectable activity when ETF is used as the electron acceptor, while its activity cannot be detected with PMS/DCIP used as the electron acceptor, even following preincubation of the sample with FAD.

DISCUSSION

This report describes the identification of seven new point mutations leading to amino acid replacements in IVD, and the characterization of the functional significance of these and two previously identified IVD mutations. Other mutations within the coding region leading to premature termination of peptide synthesis and others in the noncoding regions of the *IVD* gene causing splicing errors have also been identified and will be presented elsewhere.

Stability of the IVD Mutants. The stability of the IVD mutants has been determined by measuring IVD activity and antigen present in fibroblast extracts and through an in vitro mitochondrial import assay. Results indicate that the mutant proteins are produced in vivo, but their cellular stability varies significantly. The IVD Ala282Val mutant is the most functional of the mutants (about 8% that of wild-type enzyme activity) despite apparently reduced antigen concentration in fibroblasts. The estimated amount of this mutant relative to wild type present 60 min following in vitro mitochondrial import (Table 2) is also reduced. These results indicate that the IVD mutant has decreased stability in vivo concomitant with a more notable decrease in enzyme activity. The three-dimensional structure modeling of IVD reveals that replacement of the Ala282 side chain with that of a valine could disrupt proper alignment of side chains at the monomer−monomer interface region, leading to some perturbation in FAD binding. The β-carbon of this alanine is also close to residues which are involved in binding the FAD′ adenine base moiety (the prime designates the second monomer), including the invariant Phe283 and Phe290 which lie at a perpendicular and stacking positions relative to the adenine ring, respectively. Perturbation in FAD binding, resulting from the presence of a valine residue at position 282, could lead to loss of FAD and subsequent diminished activity and further instability of the enzyme.

Although the Western blot signal for the Arg382Leu mutant in fibroblasts is the highest among all mutants, IVD activity in patients cells harboring this mutation could not be detected. Blots from the mitochondrial import experiments were consistent with findings from patient's fibroblasts, indicating a defect in enzyme function rather than enzyme stability. Similar results for the Val342Ala mutant indicate a functionally defective IVD. The IVD Asp40Asn mutant is apparently more stable following import into mitochondria using the in vitro system as compared to its stability in the corresponding patient fibroblast cells.

Western blots of fibroblast cells, which harbor the IVD Arg363Cys and the Cys328Arg mutants, show a rather strong signal. The relative stability of these two IVD mutants following in vitro mitochondrial import is 39% and 14%, respectively. These values are a better estimate of the individual mutant proteins than estimates derived from Western blot experiments from FB 2368 fibroblast cell extracts, since both mutant proteins are likely being synthesized in the cell line. The potential formation of various hybrid IVD tetramers makes the significance of the in vivo stability data difficult to assess.

Previous fibroblast labeling studies of the IVD Leu13Pro indicated that it was appropriately imported into mitochondria and processed to a mature monomer size, but no residual IVD activity could be detected using a radiolabeled substrate (*18*). When imported into isolated mitochondria, the Leu13Pro precursor is processed to a mature form, in agreement with cell studies, but is then quickly degraded. The IVD Arg21Pro mutation was identified in a cell line which has no IVD activity as measured with the ETF fluorescence quenching assay and no IVD protein as indicated by Western blotting (see above). This mutant is also labile following import into mitochondria. The relatively rapid disappearance of IVD Leu13Pro, Arg21Pro, and Cys328Arg following import suggests that these amino acid mutations adversely affect peptide folding and/or tertiary structure stability within mitochondria. Examination of the three-dimensional crystal structure of human IVD shows that Leu13, which is at the start of α-helix A, interacts with the side chains of the conserved Leu77 and Leu81 of α-helix D. Thus, Leu13 appears to contribute to stabilizing the supersecondary structure in this region. Arg21 is also located near the same region. Its side chain is on the second turn of helix A, and its guanidino group distal nitrogens interact with the hydroxyl group of Tyr312 and one of the carboxylate oxygens of Glu84. This latter residue, which is located on α-helix D, is invariant in all ACDs.

Despite the detection of the IVD Gly170Val mutant in patient's fibroblasts, the IVD peptide could not be detected in the precursor form in the transcription/translation mixture. This is probably due to rapid degradation in the reticulocyte lysate. The vulnerability of this mutant to degradation and/or dramatic instability could be attributed to improper folding and/or improper interaction with chaperonins present in the rabbit reticulocyte extract.

E. coli Expression of IVD Mutant cDNAs. The effects of the amino acid mutations on enzyme structure and function were also evaluated by examining the production of the IVD mutants in *E. coli*. After induction with IPTG, cell extracts of the bacterial cultures were analyzed for IVD activity. The relatively higher activity of the recombinant IVD Ala282Val mutant compared to other mutants is consistent with the level of activity measured in extracts from patient fibroblasts, and is an indication of its greater stability compared to the other mutants. The significant activity present in cells producing the recombinant IVD Val342Ala and Arg382Leu mutants suggests that their role in enzyme function is not absolutely crucial.

The presence of IVD Arg21Pro, Asp40Asn, Ala282Val, Val342Ala, Arg363Cys, and Arg382Leu mutant proteins in the supernatant fraction indicates assembly of monomer into their tetramer form (Figure 4). Since the IVD Gly170Val and Cys328Arg mutants are barely detectable in the cellular supernatant, but are present in whole cells, this could be indicative of a folding defect resulting in aggregation. The dramatic diminished presence of the recombinant IVD Leu13Pro mutant in whole cells and its absence from the *E. coli* supernatant, despite the use of coexpression of bacterial GroEL/ES, imply a vulnerability to degradation and perhaps a defect early in folding (Figure 4). This is in contrast to the IVD Gly170Val and Cys328Arg mutants, which appear

to form immunoreactive protein.

The intolerance of the IVD Arg21Pro, Asp40Asn, and Arg363Cys mutants to the purification conditions used for the wild-type IVD, or the other mutants which were purified, confirms that the structural integrity of these three mutants is adversely affected by their amino acid mutations. The relatively rapid disappearance of these IVD mutants in the in vitro mitochondrial import studies suggests that these mutant proteins are vulnerable to degradation by specific mitochondrial proteases. On the other hand, the mutant recombinant proteins appear more stable or less sensitive to degradation in the prokaryotic system. Factors which could result in better stability of the recombinant IVD mutants compared to the wild type include absence of specific proteases and binding of ligands which may stabilize the protein structure, e.g., the CoA persulfide.

Spectral Analysis of Purified Recombinant IVD Mutants. Spectral scanning upon addition of substrate to the enzyme solution provides evidence for the formation of the charge-transfer complex intermediate, as distinct spectral changes establishing proper binding of substrate to the enzyme occur (Figure 6). These changes include a characteristic quenching of absorption at λ ~450 nm with the concomitant appearance of a new absorption band at λ ~580 nm (*32*−*34*). The spectra of the purified IVD Ala282Val, Val342Ala, and Arg382Leu mutants in the absence of isovaleryl-CoA are consistent with loss of FAD from the tetramers and show the presence of a CoA persulfide bound to the mutant tetramers as evident from the broad absorbency at the 650−700 nm region and the shift of the 445 nm peak from 430 nm. Since the decrease in the absorbency is along the whole 320−700 nm region in the IVD Ala282Val mutant/substrate scans, it is difficult to interpret this as indicative of the proper formation of the charge-transfer complex intermediate. The IVD Val342Ala scans showing the reduction of the flavin absorbency at λ ~430 nm and the increase in the absorption at 580 nm in the presence of saturating concentrations of isovaleryl-CoA indicate formation of a charge-transfer complex intermediate. In contrast, while the IVD Arg382Leu mutant scans show a minor red shift of the 445 nm peak region in the presence of substrate, perhaps indicating substrate binding, the insignificant reduction of absorbency near λ ~445 nm and lack of an increase in the absorbency at λ ~580 nm imply improper binding for forming the charge-transfer complex intermediate. Activity measurements of this mutant, however, indicate higher specific activity than either of the above mutants. To explain this, further elucidation of the reaction mechanism vis-à-vis C-2 proton abstraction and C-3 hydride transfer from the acyl-CoA moiety and transfer of electrons to the ultimate acceptor is required.

Kinetic Properties of Purified Recombinant IVD Mutants. The changes in the kinetic parameter values of the IVD Ala282Val mutant as compared to the wild type are similar using the ETF fluorescence and the DCIP colorimetric assays, with the K_m and V_{max} being higher and the subunit catalytic efficiency significantly lower. These results suggest that the primary cause for the dramatic decrease in the catalytic efficiency is related to a defect in substrate binding. This hypothesis is supported by molecular modeling where the β-carbon of Ala282 is found to be close to one of the phosphate group oxygens of the adenylate moiety of the FAD′, with the other phosphate group oxygen apparently being anchored by the hydroxyl group and the backbone −NH− group of Ser142′ through hydrogen bonding (serine 142 of the second monomer). The backbone carbonyl oxygen of this serine forms a hydrogen bond with the −NH− of the β-alanine moiety of the substrate that binds to the second monomer. Perturbation of these series of hydrogen bonds could lead to decreased substrate binding affinity.

The K_m of the IVD Arg382Leu is significantly lower using the PMS/DCIP assay compared to that measured with the ETF fluorescence quenching assay. In contrast, the magnitude of the decrease in the subunit catalytic efficiency of this mutant enzyme is more pronounced using the ETF fluorescence quenching assay than with the PMS/DCIP assay. This suggests that the Arg382Leu replacement more significantly affects the transfer of electrons from the IVD mutant−substrate binary complex to ETF than to PMS/DCIP. This may indicate adverse changes in the alignment of groups at the IVD−ETF docking site induced by this replacement.

Our results emphasize the importance of specific amino acids for IVD structure, FAD and substrate binding, and enzyme activity. A better description of the role of these amino acid residues requires further study, including site-directed mutagenesis with replacement of specific amino acid residues by other appropriate residues in IVD and in the homologous positions in other ACDs as well.

ACKNOWLEDGMENT

We gratefully acknowledge the many physicians who provided patient cell lines for analysis. Special thanks to Ms. Pam Becker for help with the preparation of the manuscript.

REFERENCES

1. Budd, M. A., Tanaka, K., Holmes, L. B., Efron, M. L., Crawford, M. L., and Isselbacher, K. J. (1967) *N. Engl. J. Med. 277*, 321−327.
2. Tanaka, K., Budd, M. A., Efron, M. L., and Isselbacher, K. J. (1966) *Proc. Natl. Acad. Sci. U.S.A. 56*, 236−242.
3. Sweetman, L., and Williams, J. D. (1995) in The *Metabolic and Inherited Basis of Disease* (Scriver, C., Beaudet, A. L., Sly, W., and Valle, D., Eds.) pp 1387−1422, McGraw-Hill, New York.
4. Ikeda, Y., Hale, D. E., Keese, S. M., Coates, P. M., and Tanaka, K. (1986) *Pediat. Res. 20*, 843−847.
5. Ikeda, Y., Keese, S., Fenton, W. A., and Tanaka, K. (1987) *Arch. Biochem. Biophys. 252*, 662−674.
6. Rozen, R., Vockley, J., Zhou, L., Milos, R., Willard, J., Fu, K., Vicanek, C., Low-Nang, L., Torban, E., and Fournier, B. (1994) *Genomics 24*, 280−287.
7. Ikeda, Y., and Tanaka, K. (1983) *J. Biol. Chem. 258*, 1077−1085.
8. Crane FL, B. H. (1955) *J. Biol. Chem. 218*, 717−731.
9. Aoyama, T., Souri, M., Ueno, I., Kamijo, T., Yamaguchi, S., Rhead, W. J., Tanaka, K., and Hashimoto, T. (1995) *Am. J. Hum. Genet. 57*, 273−283.
10. Kelly, D., Kim, J., Billadello, J., Hainline, B., Chu, T., and Strauss, A. (1988) *Proc. Natl. Acad. Sci. U.S.A. 85*, 4068−4072.
11. Matsubara, Y., Indo, Y., Naito, E., Ozasa, H., Glassberg, R., Vockley, J., Ikeda, Y., Kraus, J., and Tanaka, K. (1989) *J. Biol. Chem. 264*, 16321−16331.
12. Willard, J., Vicanek, C., Battaile, K. P., Vanveldhoven, P. P., Fauq, A. H., Rozen, R., and Vockley, J. (1996) *Arch. Biochem. Biophys. 331*, 127−133.
13. Kim, J. J. P., Wang, M., and Paschke, R. (1993) *Proc. Natl. Acad. Sci. U.S.A. 90*, 7523−7527.

14. Djordjevic, S., Pace, C. P., Stankovich, M. T., and Kim, J. J. P. (1995) *Biochemistry 34*, 2163−2171.
15. Tiffany, K. A., Roberts, D. L., Wang, M., Paschke, R., Mohsen, A.-W. A., Vockley, J., and Kim, J. J. P. (1997) *Biochemistry 36*, 8455−8464.
16. Andresen, B. S., Bross, P., Vianeysaban, C., Divry, P., Zabot, M. T., Roe, C. R., Nada, M. A., Byskov, A., Kruse, T. A., Neve, S., Kristiansen, K., Knudsen, I., Corydon, M. J., and Gregersen, N. (1996) *Hum. Mol. Genet. 5*, 461−472.
17. Andresen, B. S., Bross, P., Udvari, S., Kirk, J., Gray, G., Kmoch, S., Chamoles, N., Knudsen, I., Winter, V., Wilcken, B., Yokota, I., Hart, K., Packman, S., Harpey, J. P., Saudubray, J. M., Hale, D. E., Bolund, L., Kolvraa, S., and Gregersen, N. (1997) *Hum. Mol. Genet. 6*, 695−707.
18. Ikeda, Y., Keese, S., and Tanaka, K. (1985) *Proc. Natl. Acad. Sci. U.S.A. 82*, 7081−7085.
19. Naito, E., Ozasa, H., Ikeda, Y., and Tanaka, K. (1989) *J. Clin. Invest. 83*, 1605−1613.
20. Tanaka, K., Gregersen, N., Ribes, A., Kim, J., Kolvraa, S., Winter, V., Eiberg, H., Martinez, G., Deufel, T., Leifert, B., Santer, R., Francois, B., Pronicka, E., Laszlo, A., Kmoch, S., Kremensky, I., Kalaydjicva, L., Ozalp, I., and Ito, M. (1997) *Pediatr. Res. 41*, 201−209.
21. Vockley, J., Parimoo, B., and Tanaka, K. (1991) *Am. J. Hum. Genet. 40*, 147−157.
22. Mohsen, A.-W. A., and Vockley, J. (1995) *Gene 160*, 263−267.
23. Mohsen, A.-W. A., and Vockley, J. (1995) *Biochemistry 34*, 10146−10152.
24. Vockley, J., Nagao, M., Parimoo, B., and Tanaka, K. (1992) *J. Biol. Chem. 267*, 2494−2501.
25. Laemmli, U. K. (1970) *Nature 227*, 680−685.
26. Frerman, F. E., and Goodman, S. I. (1985) *Biochem. Med. 33*, 38−44.
27. Yokota, I., Saijo, T., Vockley, J., and Tanaka, K. (1992) *J. Biol. Chem. 267*, 26004−26010.
28. Battaile, K., Mohsen, A.-W., and Vockley, J. (1996) *Biochemistry 35*, 15356−15363.
29. Bross, P., Andresen, B. S., Winter, V., Krautle, F., Jensen, T. G., Nandy, A., Kolvraa, S., Ghisla, S., Bolund, L., and Gregersen, N. (1993) *Biochim. Biophys. Acta 1182*, 264−274.
30. Ikeda, Y., Okamura-Ikeda, K., and Tanaka, K. (1985) *J. Biol. Chem. 260*, 1311−1325.
31. Williamson, G., Engel, P. C., Mizzer, J. P., Thorpe, C., and Massey, V. (1982) *J. Biol. Chem. 257*, 4314−4320.
32. Massey, V., and Ghisla, S. (1974) *Ann. N.Y. Acad. Sci. 227*, 446−465.
33. Ikeda, Y., Okamura-Ikeda, K., and Tanaka, K. (1985) *Biochemistry 24*, 7192−7199.
34. Thorpe, C., Matthews, R. G., and Williams, C. H. (1979) *Biochemistry 18*, 331−337.

BI973096R